Different deformation mechanisms leading to auxetic behavior exhibited by missing rib square grid structures

P S Farrugia[*,1], R Gatt[1], E Zammit Lonardelli[1], J N Grima[1] and K E Evans[2]

Affiliation:

[1]Faculty of Science, University of Malta, Msida, MSD2080, Malta

[2]College of Engineering, Mathematics and Physical Sciences, University of Exeter, UK

Corresponding author contact information:

P S Farrugia
e-mail: pierre-sandre.farrugia@um.edu.mt
Phone: +356 2340 2178
Mobile: +356 7925 6565
Fax: +356 2133 2728

Other email contact information:

R Gatt: ruben.gatt@um.edu.mt

E Zammit Lonardelli: enrico.zammitl@gmail.com

J N Grima: joseph.grima@um.edu.mt

K E Evans: K.E.Evans@exeter.ac.uk

Abstract: An extensive investigation was carried out on the missing rib square grid structure using finite element simulations. This showed that, in the cases considered in this study, the type of deformation is primarily dependent on the ratio of the thickness of different ribs with the structure behaving like an anti-tetrachiral at particular ratios. The analysis also showed that the ability of the structure to deform predominantly through the bending of the ligament allows it to achieve much more negative values of the Poisson's ratio than previously reported. Confirmation of the numerical results was obtained through experimental methods involving the 3D printing of representative structures which were subsequently subjected to compression.

1. Introduction

When a material or structure is set in tension in most cases it elongates axially and contracts laterally. Nevertheless, not all materials and structures behave in this way. In fact there exist systems, which are usually referred to as auxetics,[1] that exhibit the unusual behavior of expanding in more than one direction when subjected to a tensile force. Interest in these structures has surged in the last decades following the publication by Lakes[2] of a method for creating auxetic foams and the work of Wojciechowski[3,4] and Evans.[5] This was driven by their enhanced properties, such as better indentation resistance[2,6,7] and larger shear stiffness,[2,8] when compared to conventional materials. As a result they have been proposed for a variety of applications ranging from core materials for curved sandwich panels[9] and shock absorbers[10] to dilator[11] and stents[12,13] for medical application. In the process, a variety of techniques were used to study them including mathematical methods,[14–17] numerical computation [18–21] and experimental.[18,19,22,23]

There exist various mechanisms that can lead to auxetic behavior. The most common include chiral structures,[3,18,24,25] rotating rigid units,[26,27] re-entrant cells,[14,28,29] and more recently perforations.[30–33] However, other mechanisms exist that can lead to auxetic behavior. One such mechanism that appears to have received relatively little attention is the missing rib model based on the square grid.[34] The structure was originally proposed as an extension of the missing rib model based on the lozenge grid.[22] However, while the missing rib lozenge grid continued to receive some attention[23,35,36] the one based on the square grid much less so.

A further interesting feature of the missing rib systems that appears to have been, until recently, mostly overlooked is the fact that they are *chiral* (where the literal sense is intended meaning that the structures are distinguishable from their mirror images). In actual fact, a close inspection shows that they carry strong resemblance to the chiral structures, with the missing rib lozenge grid looking like the tetrachiral while the missing rib square grid being akin to anti-tetrachiral (Figure 1). This similarity between the structures was hinted at in some work. For example Jiang and Li identify the missing rib lozenge grid as a chiral structure.[23] Bacigalupo and Bellis modelled the ring of the anti-tetrachiral as a rigid cross;[37] while the I-shaped perforations studied by Mizzi et al.[38], which are reminiscent of the missing rib square grid, were analyzed in terms of the behavior of the anti-tetrachiral. However, the relation between the types of structures has been explicitly stated only recently in the work of Lim.[39]

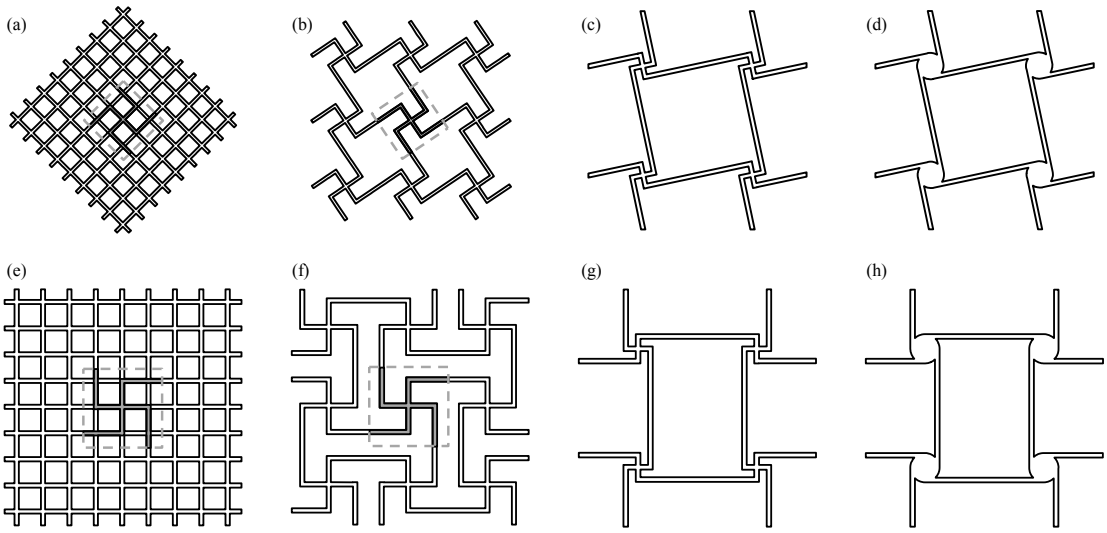

Figure 1 (a) illustrates the complete lozenge grid and (b) the resulting missing rib lozenge grid while (c) and (d) show respectively the unit cell of the missing rib lozenge grid and the tetrachiral; (e) illustrates the complete square grid and (f) the resulting missing rib square grid while (g) and (h) show respectively the unit cell of the missing rib square grid and the anti-tetrachiral.

The similarity between the missing rib square grid (henceforth referred to as square grid for simplicity) and the anti-tetrachiral suggests that the former structure should be able to deform not just through the hinging at the joints as originally proposed[22,34] but also through the rotation of the crossed-ligaments as a rigid body coupled with the bending of the ligaments joining them, i.e. the crossed-ligaments would act as a rotating centre.[40] This possibility has been mentioned by Lim,[39] who grouped the two structures under the same deformation mechanism. However, to our knowledge, there has never been an investigation to assess under what conditions the square grid will behave like the anti-tetrachiral.

Thus the aim of this work was to investigate how the various geometric parameters affect the deformation mechanism of the square grid. This was carried out through a

parametric analysis using numerical simulations. The results were then confirmed through experimental testing of representative structures produced through 3D printing.

2. Methodologies

2.1 Finite element simulations

In order to assess the possible deformation mechanisms of the square grid, finite element analysis (FEA) simulations were carried out using ANSYS APDL 13. The structure was modelled as a 2D infinite system so as to obtain the bulk properties of the material. In order to take into account the symmetry of the structure, the unit cell show in Figure 3 was used, with symmetry boundary conditions being imposed along the Ox_2 direction. This was attained by fixing the nodes that lie on one of the edges of the unit cell that is perpendicular to the Ox_2-axis so that their Ox_2 coordinate does not change while forcing the nodes on the opposite edge to have the same change in the Ox_2 coordinate. Subsequently a compressive strain was applied in the Ox_1 direction on each of the other faces by prescribing a displacement along the Ox_1-axis on the nodes.

For these simulations the element used was PLANE183, this being a higher order 2D element with 8 or 6 nodes each possessing two degrees of freedom.[41] It also has a quadratic displacement behavior (i.e. the edge of the element can take a curved shape) that is also suitable for modelling irregular meshes.[41] Plane stress was assumed and the Young's modulus was set to 1.6×10^9 Pa and the Poisson's ratio to 0.45. These values were specific to the material that was meant to be used for the experimental testing and were as average values from different dog bones that have been printed using different on-axis orientations. The automatic (smart) element sizing with the fine mesh that is available in ANSYS APDL was used. Repeated tests using different ligament thicknesses, so as to ensure mesh independency of the results,[40] indicated

that the results differed by less than 1 % from much finer meshes as shown in Figure 2. The element size was chosen such that the results obtained with it were less than 1 % different from those obtained with a finer mesh. Linear elasticity with small displacement[41] simulations were also chosen for this initial analysis in order to save on the computational time. This involves the solution of an equation of the form $[K]\{u\} = \{F\}$, where $[K]$ is the total stiffness matrix, $\{u\}$ is the nodal displacement vector and $\{F\}$ is the total reaction and applied load vector. Subsequently some nonlinear simulations were carried out to confirm the initial results obtained in this way.

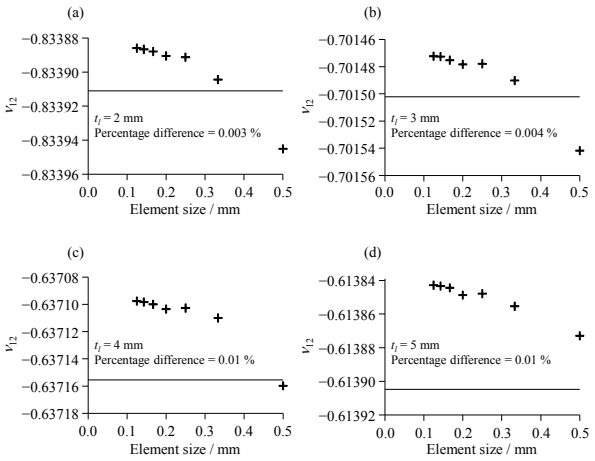

Figure 2 A sample of the mesh convergence tests that were carried out. The straight line indicates the value obtained using automatic (smart) element sizing while the plus signs indicate the values obtained by when choosing the element size. The dimensions of the structures are $l_1 = l_1 = 25$ mm, $r' = 5$ mm, $t_r = 2$ mm while t_l is given on the graph.

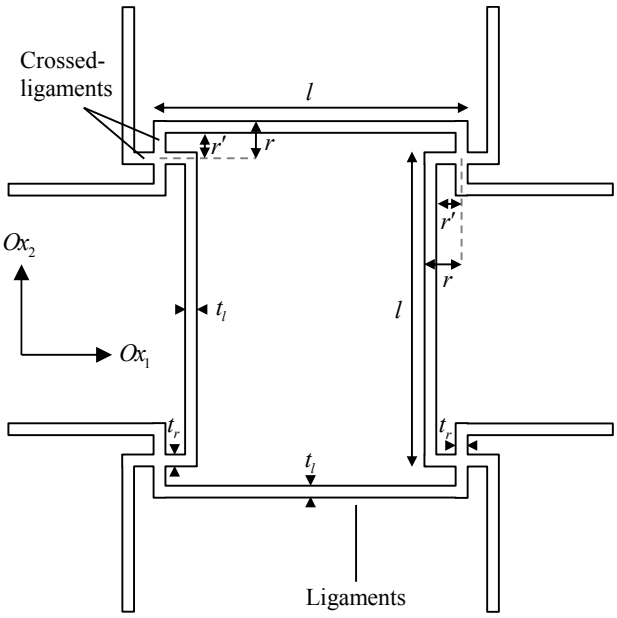

Figure 3 The physical representation of the parameters used in the analysis.

The parameters that were varied are illustrated in Figure 3. For simplicity the dimensions of the ligaments joining the "nodes" (also referred to as rotating centers[40])or crossed-ligaments was taken to be the same for both direction. The same holds for the dimensions of the crossed-ligaments. Linear simulations were then carried out for the ligament length l varying from 10 mm to 50 mm in steps of 5 mm while the ligament thickness t_l and the crossed-ligaments thickness t_r were both assigned values between 0.2 mm and 40 mm in increments of 0.2 mm. Regarding the crossed-ligament, initial investigations indicated that it is better to vary the distance from the middle of the crossed-ligaments to the inner edge of the ligament r' rather than to the outer edge r. The values of r' were thus varied between 1 mm and 24 mm in steps of 1 mm.

Not all resulting geometries were tesselatable because the ligaments could overlap with cross-ligaments if $r-t_l-t_r/2\leq 0$. In order to avoid this and to allow space for the deformation of the ligament, structures for which $r-t_l-t_r/2\leq 1$ mm were not considered. Similarly cases where $l-2r\leq 1$ mm were not considered so as to avoid that adjacent

crossed-ligaments overlap. Furthermore, in order to reduce the stresses at sharp bends, a slight curvature that was relatively small compared to the dimensions of the structure being considered was introduced at each corner or joint.

As will be discussed in more detail later on, the parametric investigation showed that the structure could deform both through the bending of the crossed-ligaments and through bending of the ligaments. Thus two representative structures which deform predominantly through only one of these mechanisms were selected and analyzed using non-linear simulations, up to 3.5 % strain. The one deforming through the hinging of the joints had the following dimensions l = 14 mm, r = 6 mm, t_l = 3 mm and t_r = 1.5 mm while the one deforming through the bending of the ligaments had the same l and r while t_l = 1.5 mm and t_r = 3 mm. Data for the non-linear behavior of the material was obtained by analyzing a dog bone made from the same filament that was used to print the structures for testing.

2.2 Production of the samples and measurements made

A sample of the representative structures that deform predominantly through only one of the mechanisms identified in the parametric analysis were 3D printed using an Ultimaker 3 FFF (fused filament fabrication) 3D printer. The structures were printed using Ultimaker PLA (polylactic acid) filament with the extruder temperature set to 205 °C and the bed temperature set to 60 °C. The infill density was set to 100 % whilst the layer height was set to 0.2 mm. To prevent the risk of warping, Magigoo® 3D printing adhesive was used on the printing bed.

The samples produced (Figure 4) where made up of 4 by 4 unit cells and had a depth of 15 mm. As can be noted from Figure 4, in order to distribute the stress on the whole

length of the structure, a bar of width 5 mm was added along the faces perpendicular to the loading direction.

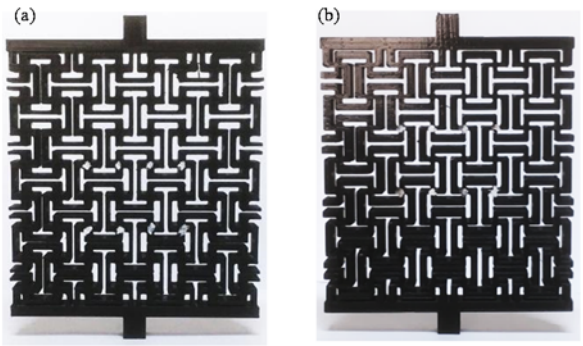

Figure 4 The samples used for the experimental measurements with (a) deforming through the bending of the ligaments while (b) through the bending of the crossed-ligaments.

Once printed, the structures were tested under compression using a Testometric universal loading machine (M350-20CT) with a 1000 N load cell (Serial Number: 31931). One set of two white markers where applied in the axial direction and two sets (each containing two) of white markers in the transverse direction. A compressive strain of around 3.5 % was applied with the deformation being recorded with a duly calibrated Mesh Physique Videoextensiometer camera. The change in lengths, measured for a central unit cell,[42] was monitored using the pattern recognition feature found within the Videoextensiometer software. This resulted in one reading for the axial direction and two readings for the transverse direction from which the Poisson's ratio could be determined.

3. Results and discussion

3.1 Linear finite element simulations

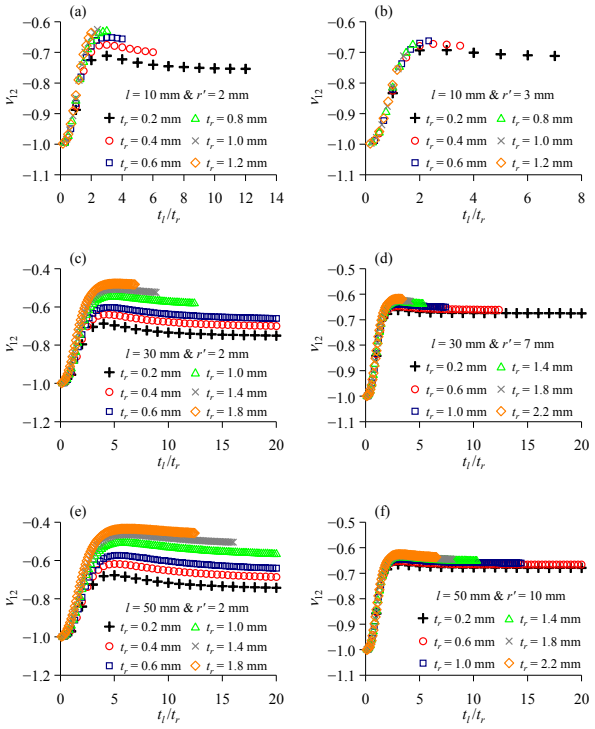

Figure 5 The variation of the Poisson's ratio with the ratio t_l/t_r for different values of l, r' and t_r.

The variations of Poisson's ratio with the ratio t_l/t_r for different l, r' and t_r are shown in Figure 5. Parameter values were chosen so that the graphs obtained provide a comprehensive overview of the observed behavior of ν_{12}. Furthermore, given the symmetry of the structure along the primary axes, only loading in the Ox_1 direction was considered.

As can be noted from Figure 5 there appears to be a prevalent general trend: When the ratio t_l/t_r is small, i.e. less than around 0.5, the Poisson's ratio is close to −1 indicating that the structure is behaving like the anti-tetrachiral with the crossed-ligaments rotating

as a rigid unit. The way the structure behaves in this region is illustrated in Figure 6(a). As the t_l/t_r increases beyond around 0.5, the Poisson's ratio also starts increasing and continues to do so until the t_l/t_r ratio achieves a value of around 2 where ν_{12} attains a maximum. In this region the deformation of both the ligaments and the crossed-ligaments is important as can be noted from Figure 6(b). On increasing the ratio of the thicknesses further, the value of the Poisson's ratio stays approximately constant or decreases slightly. It can be observed from Figure 6(c) that for large values of the ratio t_l/t_r the structure deforms prevalently through the bending of the crossed-ligaments.

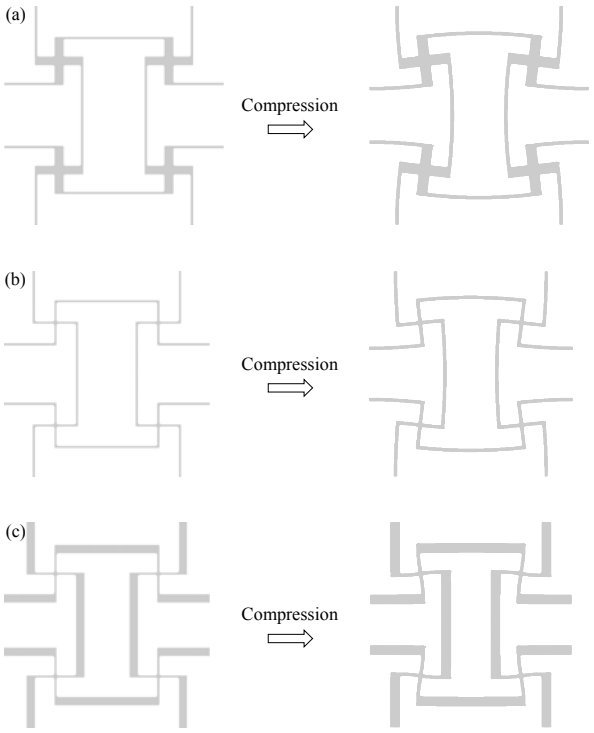

Figure 6 The deformed shapes of the structure for different geometric dimensions. In (a) only the ligaments deform with l = 50 mm, r' = 10 mm, t_l = 1 mm while t_r = 4 mm; in (b) both the ligaments and the crossed-ligaments deform with l = 50 mm, r' = 10 mm, while $t_l = t_r$ = 1 mm; and in (c) only the crossed-ligaments deform with l = 50 mm, r' = 10 mm, t_l = 4 mm while t_r = 1 mm.

Further observation of Figure 5 suggests that the mode of deformation is mostly independent of the ligament length. However it depends to some extent on r' and t_r. In fact when t_r increases, the maximum attained by the Poisson's ratio also increases. This is particularly evident for small r' (refer to Figure 2 for parameters) where the increase of the maximum ν_{12} is more pronounced. On the other hand as r' increases the behavior of the Poisson's ratio for different t_r tends to converge.

The analysis of these results clearly indicates that the behaviour of square chiral when uniaxial loaded is more complex than previously reported. There are two mechanisms that can act: the bending of the ligaments and the bending of the crossed-ligaments. The results indicate that the former leads to a more negative Poisson's ratio than the latter. An explanation for this can be found in the fact that when the dominant mechanism is the bending of the ligaments, the angle between the crossed-ligaments does not change. Thus the deformation along the loading axis is transmitted in full to the orthogonal axis. On the other hand, when the crossed-ligaments bend, the angle at their centre changes so that the effective rotation of the "node" is smaller. This makes the on-axis strain larger than the lateral strain so that the Poisson's ratio is less negative. Thus, the extent to which the crossed-ligaments act as a rigid rotating centre is an important determination factor in the resultant Poisson's ratio as has already been observed in the case of the anti-chiral structures with random circular nodes.[41] This observation is also akin to the findings of Pozniak et al.[43] who report that increasing the stiffness of the joints of their kagome lattice or replacing the Y-type joints with Δ-type joints (which can be expected to be stiffer) decreases the Poisson's ratio.

Interestingly enough, the transition region between the two mechanisms occurs prevalently along a specific range of the ratio of the thicknesses of the ligaments. This

feature can be very important from a production point of view since for the same geometric size of the unit cell it allows for a very easy way to fine tune the behaviour of the structure. Another important aspect of the behaviour of the material is that when r' is large the variation of ν_{12} with t_l/t_r is basically the same irrespective of the other geometric dimensions. Thus the Poisson's ratio attained by the structure is rather insensitive to production defects for structures with t_l/t_r greater than 2. For structures with t_l/t_r smaller than 2 the ν_{12} would only be sensitive to the ratio of t_l/t_r. The similarity of behaviour of the structure for different parametric values can also allow for the decrease of the material used in building the system while still retaining the same Poisson's ratio.

3.2 Experimental results and nonlinear finite element simulations

In order to investigate further the results obtained, two structures that deform predominantly by one of the two mechanisms were studied in more depth by carrying out non-linear finite element simulations. At the same time a 3D printer was used to produce these structures that were subsequently subject to compressive testing as described in Section 2. Comparison of the results obtained is shown in Figures 7 and 8. It can be clearly observed that the strains measured experimentally and those obtained from the nonlinear finite element simulations are in excellent agreement. In fact for the structure shown in Figure 7, the Poisson's ratio determined experimentally was −0.940, that obtained using nonlinear FEA simulations was −0.944 while that obtained using linear FEA simulations was −0.946. Similar, in the case of the structure shown in Figure 8 the Poisson's ratio determined experimentally was −0.601, that obtained using nonlinear FEA simulations was −0.632 while that obtained using linear FEA simulations was −0.637. The agreement between the experimental and numerical values

indicates that both linear and nonlinear FEA simulation are able to predict with good precision the Poisson's ratio for these structure. This gives further confidence to the parametric analysis carried out in the previous section.

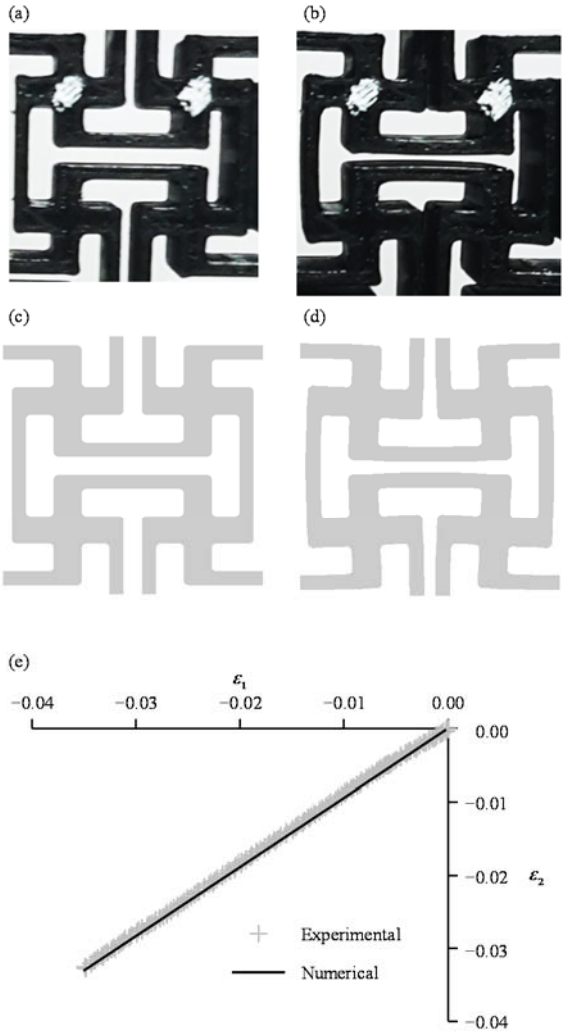

Figure 7 (a) and (b) illustrate respectively a unit cell of the undeformed and deformed 3D printed structure when the deformation is dominated by the bending of the ligaments; (c) and (d) show the corresponding system obtained using nonlinear FEA while (e) shows the variation of ε_2 with ε_1. Here l = 14 mm, r = 6 mm, t_l = 1.5 mm and t_r = 3 mm while compression is applied along the vertical direction.

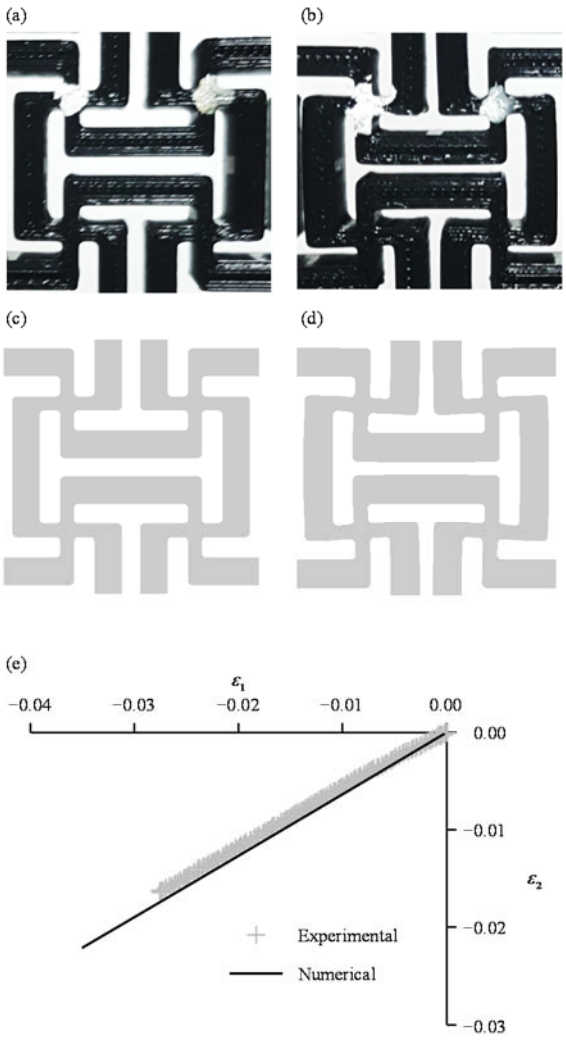

Figure 8 (a) and (b) illustrate respectively a unit cell of the undeformed and deformed 3D printed structure when the deformation is dominated by the bending of the crossed-ligaments; (c) and (d) show the corresponding system obtained using nonlinear FEA; while (e) shows the variation of ε_2 with ε_1. Here l = 14 mm, r = 6 mm, t_l = 3 mm and t_r = 1.5 mm while compression is applied along the vertical direction.

4. Conclusion

This work analyses in depth the deformation mechanics present in the missing rib square grid structure. A parametric analysis of the behavior using finite element analysis revealed that two mechanisms can act, one involving the bending of the

ligament and the other the bending of the crossed-ligaments. The results show that both mechanisms can lead to auxetic behavior. However, the bending of the ligaments allows the attainment of more negative Poisson's ratio. The relative contribution of each mechanics was found to be primarily dependent on the ratio of the thickness of the ligament to that of the crossed-ligaments. When the thickness of the ligament is small compared to that of the crossed-ligaments, the bending of the ligaments dominates and the deformation of the square grid is akin to that of the anti-tetrachiral. At the other extreme, when the thickness of the ligaments is small compared to that of the crossed-ligaments, bending of the crossed-ligaments dominates. In between there is a transition region that appears to occur over the same range of the ratio of the thicknesses irrespective of the other physical dimensions. Experimentally determined Poisson's ratio for representative structures were in good agreement with both the nonlinear and the linear finite element results. Thus the work showed that the deformation of the square grid is richer than previously reported. In addition the dependence on the structure parameters that is being reported provides for new ways of fine tuning its Poisson's ratio. It also provides for regions in the parametric values where the Poisson's ratio is rather insensitive to some or all of the physical dimensions of the structure, a feature that can be very important from a production point of view.

Acknowledgment

This research has been carried out using computational facilities procured through the European Regional Development Fund, Project ERDF-080 'A supercomputing laboratory for the University of Malta' (http://www.um.edu.mt/research/scienceeng/erdf_080) and those procured through the University of Malta Academic Work Resources Fund.

References

[1] K. E. Evans, *Endeavour* **1991**, *15*, 170.

[2] R. Lakes, *Science* **1987**, *235*, 1038.

[3] K. W. Wojciechowski, *Mol. Phys.* **1987**, *61*, 1247.

[4] K. W. Wojciechowski, *Phys. Lett. A* **1989**, *137*, 60.

[5] K. E. Evans, M. A. Nkansah, I. J. Hutchinson, S. C. Rogers, *Nature* **1991**, *353*, 124.

[6] A. Alderson, *Chem. Ind.* **1999**, *17*, 384.

[7] K. E. Evans, K. L. Alderson, *Eng. Sci. Educ. J.* **2000**, *9*, 148.

[8] A. Alderson, K. L. Alderson, *Proc. Inst. Mech. Eng. Part G J. Aerosp. Eng.* **2007**, *221*, 565.

[9] K. E. Evans, *Compos. Struct.* **1991**, *17*, 95.

[10] T. Bückmann, R. Schittny, M. Thiel, M. Kadic, G. W. Milton, M. Wegener, *New J. Phys.* **2014**, *16*, 033032.

[11] R. E. Moyers, *Dilator for Opening the Lumen of a Tubular Organ*, Google Patents, **1992**.

[12] R. Gatt, R. Caruana-Gauci, D. Attard, A. R. Casha, W. Wolak, K. Dudek, L. Mizzi, J. N. Grima, *Phys. Status Solidi B* **2014**, *251*, 321.

[13] M. N. Ali, I. U. Rehman, *J. Mater. Sci. Mater. Med.* **2011**, *22*, 2573.

[14] L. J. Gibson, M. F. Ashby, *Cellular Solids: Structure and Properties*, Cambridge University Press, Cambridge, **1999**.

[15] D. Prall, R. S. Lakes, *Int. J. Mech. Sci.* **1997**, *39*, 305.

[16] Z. Rueger, D. Li, R. S. Lakes, *Phys. Status Solidi B* **2017**, *254*, 1600840.

[17] K. W. Wojciechowski, *J. Phys. Math. Gen.* **2003**, *36*, 11765.

[18] A. Alderson, K. L. Alderson, D. Attard, K. E. Evans, R. Gatt, J. N. Grima, W. Miller, N. Ravirala, C. W. Smith, K. Zied, *Compos. Sci. Technol.* **2010**, *70*, 1042.

[19] D. Li, J. Ma, L. Dong, R. S. Lakes, *Phys. Status Solidi B* **2017**, *254*, 1600785.

[20] W. G. Hoover, C. G. Hoover, *Phys. Status Solidi B* **2005**, *242*, 585.

[21] J. N. Grima, R. Gatt, A. Alderson, K. E. Evans, *Mol. Simul.* **2005**, *31*, 925.

[22] C. W. Smith, J. N. Grima, K. E. Evans, *Acta Mater.* **2000**, *48*, 4349.

[23] Y. Jiang, Y. Li, *Adv. Eng. Mater.* **2017**, *19*, 1600609.

[24] R. Lakes, *J. Mater. Sci.* **1991**, *26*, 2287.

[25] R. Gatt, D. Attard, P.-S. Farrugia, K. M. Azzopardi, L. Mizzi, J.-P. Brincat, J. N. Grima, *Phys. Status Solidi B* **2013**, *250*, 2012.

[26] J. N. Grima, K. E. Evans, *J. Mater. Sci. Lett.* **2000**, *19*, 1563.

[27] J. N. Grima, P. S. Farrugia, R. Gatt, D. Attard, *Phys. Status Solidi B* **2008**, *245(3)*, 521.

[28] I. G. Masters, K. E. Evans, *Compos. Struct.* **1996**, *35*, 403.

[29] K. E. Evans, A. Alderson, F. R. Christian, *J. Chem. Soc. Faraday Trans.* **1995**, *91*, 2671.

[30] A. Slann, W. White, F. Scarpa, K. Boba, I. Farrow, *Phys. Status Solidi B* **2015**, *252*, 1533.

[31] H. Mohanraj, S. L. M. Filho Ribeiro, T. H. Panzera, F. Scarpa, I. R. Farrow, R. Jones, A. Davies-Smith, C. D. L. Remillat, P. Walters, H.-X. Peng, *Phys. Status Solidi B* **2016**, *253*, 1378.

[32] K. Bertoldi, P. M. Reis, S. Willshaw, T. Mullin, *Adv. Mater.* **2010**, *22*, 361.

[33] J. T. B. Overvelde, S. Shan, K. Bertoldi, *Adv. Mater.* **2012**, *24*, 2337.

[34] N. Gaspar, X. J. Ren, C. W. Smith, J. N. Grima, K. E. Evans, *Acta Mater.* **2005**, *53*, 2439.

[35] R. Magalhaes, P. Subramani, T. Lisner, S. Rana, B. Ghiassi, R. Fangueiro, D. V. Oliveira, P. B. Lourenco, *Compos. Part Appl. Sci. Manuf.* **2016**, *87*, 86.

[36] P. Subramani, S. Rana, D. V. Oliveira, R. Fangueiro, J. Xavier, *Mater. Des.* **2014**, *61*, 286.

[37] A. Bacigalupo, M. L. D. Bellis, *Compos. Struct.* **2015**, *131*, 530.

[38] L. Mizzi, K. M. Azzopardi, D. Attard, J. N. Grima, R. Gatt, *Phys. Status Solidi RRL – Rapid Res. Lett.* **2015**, *9*, 425.

[39] T.-C. Lim, *Phys. Status Solidi RRL – Rapid Res. Lett.* **2017**, *11*, 1600440.

[40] A. A. Pozniak, K. W. Wojciechowski, *Phys. Status Solidi B* **2014**, *251*, 367.

[41] ANSYS Inc., *ANSYS 13 Mechanical APDL Documentation*, **2011**.

[42] J. N. Grima, L. Mizzi, K. M. Azzopardi, R. Gatt, *Adv. Mater.* **2016**, *28*, 385.

[43] A. A. Pozniak, J. Smardzewski, K. W. Wojciechowski, *Smart Mater. Struct.* **2013**, *22*, 084009.